Separation Science and Technology
Publication details, including instructions for authors and subscription information:
http://www.informaworld.com/smpp/title~content=t713708471

Computer Simulation Studies of the Storage of Methane in Microporous Carbons

Mary J. Bojan[a]; Richard van Slooten[b]; William Steele[c]
[a] DEPARTMENT OF CHEMISTRY, 152 DAVEY LABORATORY, PENN STATE UNIVERSITY, UNIVERSITY PARK, PENNSYLVANIA [b] LINDE DIVISION, TONAWANDA, NEW YORK [c] DEPARTMENT OF CHEMISTRY, 152 DAVEY LABORATORY, PENN STATE UNIVERSITY UNIVERSITY PARK, PENNSYLVANIA

To cite this Article Bojan, Mary J. , van Slooten, Richard and Steele, William(1992) 'Computer Simulation Studies of the Storage of Methane in Microporous Carbons', Separation Science and Technology, 27: 14, 1837 — 1856
To link to this Article: DOI: 10.1080/01496399208019453
URL: http://dx.doi.org/10.1080/01496399208019453

SEPARATION SCIENCE AND TECHNOLOGY, **27**(14), pp. 1837–1856, 1992

Computer Simulation Studies of the Storage of Methane in Microporous Carbons

MARY J. BOJAN
DEPARTMENT OF CHEMISTRY
152 DAVEY LABORATORY
PENN STATE UNIVERSITY
UNIVERSITY PARK, PENNSYLVANIA 16802

RICHARD VAN SLOOTEN
LINDE DIVISION
PRAXAIR
175 EAST PARK DRIVE, P.O. BOX 44, TONAWANDA, NEW YORK 14151-0044

WILLIAM STEELE
DEPARTMENT OF CHEMISTRY
152 DAVEY LABORATORY
PENN STATE UNIVERSITY
UNIVERSITY PARK, PENNSYLVANIA 16802

Abstract

Simulated isotherm and energies of adsorption are reported for methane in a number of model porous solids at 300 K. The solids are made up of graphite basal planes arranged to make either parallel-walled slit pores or pores of triangular cross section. The limiting low coverage behavior was characterized by direct calculations of Henry's law constants and average gas–solid energies for the pore systems considered. The isotherms were evaluated for pressures ranging up to 50 atm by utilizing the Widom particle insertion algorithm. The simulations and calculations were carried out for a range of pore sizes and, in the case of the triangular cross-section, for a range of apex angles in the isosceles triangles considered. Methane storage capacities of model solids were evaluated for values of the porosity based on two different choices of pore wall thickness. Although it is shown that adsorption is not limited to monolayer formation under these conditions, capacities obtained are not sufficiently large to meet or exceed the commonly stated requirements for use in automotive fuel storage.

1. INTRODUCTION

There has recently been a rapid growth in the number and diversity of computer simulation studies of the properties of fluids in porous media. For the most part, this work has been limited to simple geometries such as parallel-walled slits (*1*, *2*) or straight-walled cylindrical pores (*3*). [Zeolites are an exception to this generalization (*4*)]. In addition, most simulations are carried out at temperatures where the sorbed fluid can condense to a dense liquidlike phase, i.e., at temperatures below the bulk critical temperature of the fluid. Nevertheless, there is practical interest in simulations at considerably higher temperatures. For example, the sorption of methane in porous media at room temperature is being investigated as a potential method for the storage of natural gas as an automotive fuel. Here, the questions to be answered include: How much can be stored at some convenient pressure (500 psi is often chosen)?; What is the optimum pore structure for such adsorption?; How much heat is evolved upon pore filling (and absorbed upon pore emptying)?

This paper describes computer simulations of the adsorption of methane in slit pores, with parallel walls of varying separation, and with triangular cross-sections. This study differs from a similar investigation of parallel-walled slits by Tan and Gubbins (*1*) in that (a) molecular dynamics was used rather than Monte Carlo, giving us the opportunity to evaluate diffusional behavior, which will be reported in a subsequent publication; and (b) adsorption isotherms were evaluated by using the method of particle insertion (also known as the potential distribution algorithm) (*5*). Here primary emphasis will be placed on the isotherms and heats generated for methane adsorbed in various pore geometries but at a fixed temperature of 300 K. In addition to the simulations, the adsorption Henry's law constant K_H and the average energy of an isolated molecule in the pore were evaluated by direct integration. The usual definition of K_H for an adsorbed gas was used (*6*); namely,

$$K_H = \frac{1}{kT} \int_V [\exp[-u_s(\mathbf{r})/kT] - 1]\, d\mathbf{r} \tag{1.1}$$

where V is the pore volume and $u_s(\mathbf{r})$ is the interaction energy of a gas molecule at point $\mathbf{r}$ inside the pore with the solid adsorbent.

The average potential energy per particle of the adsorbed atoms $\tilde{E}_a$ is readily calculated from the simulations. It also can be expressed as a power series:

$$\tilde{E}_a = \langle u_1 \rangle + \frac{n_a}{1!} \langle u_2 \rangle + \frac{n_a^2}{2!} \langle u_3 \rangle + \cdots \tag{1.2}$$

where n_a is the number of adsorbed molecules and $\langle u_1 \rangle$ is the average energy of a single molecule in the pore, and is related to the Henry's law constant by

$$\langle u_1 \rangle = kT - k\left(\frac{d \ln K_H}{d(1/T)}\right) \tag{1.3}$$

In Eq. (1.3), $\langle u_2 \rangle$ and $\langle u_3 \rangle$ are related to the average potential energies of two and three molecules in the pore. Note that the isosteric heat of adsorption $q_{st}(n_a)$ is defined as

$$q_{st} = \bar{H}_g - \overline{H}_a \tag{1.4}$$

$$= \left[kT - \bar{E}_a - n_a\left(\frac{\partial \bar{E}_a}{\partial n_a}\right)_T\right]N_0 \tag{1.5}$$

where the bars denote partial molal quantities (per molecule), $\bar{H}_g$ is the (ideal) gas enthalpy per molecule, and N_0 is Avogadro's number. In this way, one finds

$$q_{st}(n_a) = \left[kT - \langle u_1 \rangle - 2\frac{n_a}{(\ell)}\langle u_2 \rangle - 3\left(\frac{n_a}{(\ell)}\right)^2 \langle u_3 \rangle - \cdots\right]N_0 \tag{1.6}$$

Values of $\langle u_1 \rangle$ were calculated during the evaluation of K_H (see also Tan and Gubbins).

The combination of the isotherm and energy data produces a rather complete description of the thermodynamics of methane adsorption at room temperature in graphitic pores of particular cross-sections. The varying pore dimensions selected for study allow one to deduce an optimum pore size for adsorption. The idea behind the studies of pores of triangular cross-section is that technical samples of partially graphitized carbon black often have pores with walls made up of basal planes which have been deformed by cracking. The pores that result are slit-like, but rather than having parallel walls, they exhibit triangular cross-sections. The cross-sections of such pores are idealized here into isosceles triangles. Simulations have been carried out using various values of the base length and of the vertex angle. Although large vertex angles would appear to be the best choice for modeling nearly parallel walled slits, we have varied this angle in an attempt to locate the optimum pore shape for adsorption, consistent with an isosceles triangular cross-section and an infinite length. The results of this calculation will be presented, together with computed isotherms and energies of adsorption for two pores with vertex angles of 150 and 100°.

2. SIMULATION DESCRIPTION

In computer studies, a proper choice of intermolecular interactions is crucial to the realism of the simulation. At the high temperature used in this study, the difference between tetrahedral and spherical symmetry of the methane molecules is unimportant, which allows us to model the CH_4–CH_4 energies by Lennard–Jones 12–6 functions with coefficients chosen to fit the experimental bulk second virial coefficients (*7*). Values are listed in Table 1. Since theory indicates that the well depths for pairs of atoms or molecules adsorbed on the surface of a solid should be reduced by ~15%, an appropriately smaller value was used in this simulation for the well-depths of such pairs. A second simplification can be made by neglecting the small periodic variation in methane–graphite basal plane energy due to the atomic nature of the substrate. Consequently, the gas–solid potential, which was obtained from the assumption of a pair-wise sum (over the solid) of CH_4–C site energies, can be written as

$$u_s(z_\alpha) = \frac{2\pi\epsilon_{gs}\sigma_{gs}^2}{a_s} \sum_i \sum_\alpha \left\{ \frac{2}{5}\left(\frac{\sigma_{gs}}{z_{\alpha i}}\right)^{10} - \left(\frac{\sigma_{gs}}{z_{\alpha i}}\right)^4 \right\} \tag{2.1}$$

where the sum over α denotes the sides of the pore and the sum over i denotes the ith layer in the αth pore wall, with $z_{\alpha i} = z_\alpha + id$, d = distance between graphite carbon layers (= 3.40 Å), a_s = area per C in the basal plane, and z_α = distance between the CH_4 molecule and the pore wall. The summations over graphite planes have been accurately approximated by closed form expressions which are used in this work (*8*). The well-depth and size parameters, ϵ_{gs} and σ_{gs}, were chosen to fit (*9*) the experimental data (*10*) for the Henry's law constants of methane on graphite. Values are given in Table 1 together with ϵ_{1s}, the minimum in the CH_4–graphite potential (for a single wall) and σ_{1s}, the position of the zero in the CH_4–graphite curve.

TABLE 1
Parameters of the Interaction Energies

		ϵ/k (deg K)	σ (Å)
Pairwise	CH_4–CH_4	148 (126, first layer)	3.82
Pairwise	CH_4–C site	66	3.60
Total	CH_4–solid	−1424 (minimum energy)	3.57 (gas–solid distance for zero energy)

These potential functions were used in numerical calculations of the Henry's law constant (Eq. 1.1) and the average energy of a single adsorbed atom $\langle u_1 \rangle$. Simulations of the adsorbed methane at high pore densities were performed using a predictor-corrector algorithm with a timestep of 3.3×10^{-15} s together with the isokinetic equations of motion due to Evans and Hoover (*11*). Run times to achieve equilibrium were generally 30 ps, and subsequent data gathering at intervals of 10 timesteps was carried out for 10,000 additional timesteps (33 ps). (Equilibration times of 17 ps were used in the runs for the 14.8 Å slit pore.) Quantities simulated included the energy of the adsorbed molecules, subdivided into gas–solid and gas–gas terms and, on occasion, into energies within volume elements at various distances from the walls in the slit pores.

For the parallel-walled pores, seven values of Z_p, the pore width, were taken ranging from 11.1 to 29.5 Å where the width is measured from the center of the carbon atoms which make up the basal planes of graphite; the pore dimensions in the simulation box were set at $Z_p \times 59.0$ Å $\times 63.9$ Å. (Of course, the use of periodic boundary conditions means that the pore is effectively infinite in all dimensions except z. The number of adsorbed molecules in these pores ranged up to 400.)

For the triangular slit pores, a simple modeling of the gas–solid interaction was used in which it was assumed that each of the three pore walls was made up of a semi-infinite stack of graphite basal planes. These stacks are arranged to give a pore cross-section with the desired size and shape. Of course, the use of semi-infinite planes for each wall means that they overlap at the corners. This produces an interaction which is somewhat too strong at the corners. Considering the level of knowledge of the actual situation at the corners and the simplifications that result from this approach, the errors are felt to be acceptable.

The most important (and most elusive) aspect of the calculation was that of the chemical potential of the adsorbed molecules. This leads directly to a simulation of the adsorption isotherm which here will be given as molecules adsorbed per unit pore volume as a function of the pressure (in atmospheres). The chemical potential calculation was done using the particle insertion method of Widom. Since the detailed derivation of this algorithm has been given elsewhere (*5*), only a brief description will be given here. This method involves the insertion of an imaginary (noninteracting) particle into a "real" configuration, followed by calculation of the Boltzmann factor (BFT) for this added test particle. Thus,

$$\text{BFT} = e^{-[u_s(r_t)/kT + u(r_t)/kT]} \tag{2.2}$$

where $u(r_t)$ is the interaction energy of the test particle with the real molecules in the system and $u_s(r_t)$ is the interaction energy of the test particle

with the pore walls. If $\langle BFT\rangle_{N-1}$ denotes the Boltzmann factor of the imaginary test particle averaged over configurations of $N - 1$ particles, it has been shown that

$$e^{\mu/kT} = \Lambda^3\rho(\mathbf{r})/\langle BFT\rangle_{N-1} \tag{2.3}$$

where $\Lambda = h/\sqrt{2\pi mkT} = 0.252$ Å for methane at 300 K and $\rho(\mathbf{r})$ is the local density at the test particle position $\mathbf{r}$. The pressure is readily obtained using

$$\ln\left(\frac{p}{kT}\right) = -\ln\left[\frac{\langle BFT\rangle_{N-1}}{\rho(\mathbf{r})}\right]^{12} \tag{2.4}$$

When a system is in equilibrium, the chemical potential is constant at any (or many) points in the system. To prove that this was indeed the case in these simulations, the chemical potential was calculated in several regions of the parallel-walled pore of width 14.8 Å. To do this, the pore volume was subdivided in the direction perpendicular to the pore walls. Each element, centered at z_i, was of width $\Delta z = 0.5$ Å. Particles were inserted randomly in these small volumes [whose area ($\mathfrak{a}$) is equal to the area of the simulation cell] and $\langle BFT\rangle_{N-1,z_i}$ was evaluated for each configuration. The local density $\rho(r)$ was taken to be the density in the volume element so that

$$\rho_j(z_j) = n_j/\mathfrak{a}\Delta z$$

where n_j is the number of molecules in the element centered at z_i for the jth configuration. The average local density as a function of z can easily be obtained by summation:

$$\overline{\rho(z_i)} = \frac{\sum_{j=1}^{M} \rho_j(z_i)}{M}$$

where M is the total number of configurations used. Similarly, the local energy per particle is a function of z. A local energy can be simulated which is

$$E_{tot}(z) = \frac{\sum_{j=1}^{M}\sum_{i=1}^{NP} u_s^{ij}(z) + u_{gg}^{ij}(z)}{M*NP} \tag{2.5}$$

where $u_s^{ij}(z)$ and $u_{gg}^{ij}(z)$ are the gas–solid and gas–gas interactions of the ith molecule in the jth configuration at z, and NP is the total number of particles in the simulation.

Since the positions of the test particles are distributed at random throughout the volume element, it is possible that a test particle would be inserted on top of a real particle (especially in the high density regions). A situation such as this results in a small value for BFT, corresponding to a large repulsive interaction. Since these do not contribute significantly to the average, it is often necessary to perform a large number of particle insertions—as many as 10^6—to get a precise value for the chemical potential. To assure good statistics in this calculation, we insisted that there be a fixed number of "good" particle insertions, i.e., particles which found holes and contribute significantly to the BFT. If a test particle contributed less than 8.3×10^{-7} [corresponding to $(u_{gg} + u_s)/kT = 14$] to the BFT, it was not counted as a "good" particle insertion. (Of course, the total number of "good" and "bad" particle insertions was counted for each configuration and then used to normalize the average BFT.)

Table 2 lists the average values of the chemical potential calculated in this way by using 18 values of z_i for each coverage. The range of the average number of tries needed to get a sufficient number of "good" particle insertions in each configuration is also given. In general, the number of attempted particle insertions in the dense regions near the pore walls was approximately twice that needed in regions in the middle of the pore. The total number of particles inserted is approximately equal to the number of tries times the number of configurations used. These values are listed in Table 2 for simulations with 160, 240, and 320 particles and a pore width of 14.8 Å.

In addition to this calculation of the local chemical potential, a global chemical potential was calculated. This was done by inserting test particles randomly throughout the entire pore volume. We insisted on having 4000 successful particle insertions for each configuration, and then averaged

TABLE 2
Comparison of Local and Global Chemical Potentials in the Pore of Width 14.8 Å

NP	Number of successful particle insertions per configuration	Number of configurations saved	Number of attempted particle insertions (range)	Average of local μ/kT	Global μ/kT
160	500	1,000	5×10^5 to 1×10^6	-12.60 ± 0.14	-12.4
240	200	10,000	3×10^6 to 6×10^6	-11.99 ± 0.11	-11.8
320	500	1,000	1×10^6 to 2.8×10^6	-11.32 ± 0.16	-11.2

over the 1000 configurations collected. Since the particles were distributed throughout the pore, the density used was simply the total number of particles divided by the volume of the simulation cell. By calculating the average local chemical potential, the global and local chemical potentials can be compared. Table 2 lists these two values for 3 simulations (together with supporting information), and the results agree quite well. Table 3 lists the average number of particle insertions per configuration needed to get 4000 successful tries as well as the global density of the pore and chemical potential. The pressure can be calculated from the chemical potential. To obtain an adsorption isotherm, n_a is calculated by subtracting the number of molecules in the gas phase (n_{gas}) from the total number of molecules in the simulation (NP)

$$n_a = NP - n_{gas} \tag{2.6a}$$

TABLE 3
Simulation Results

Z_p (Å)	N_p	Average tries for 4000 insertions	Pore density (molecules/Å^3)	μ/kT
11.1	160	20×10^3	3.83×10^{-3}	−12.98
	240	39×10^3	5.74×10^{-3}	−12.15
	320	108×10^3	7.66×10^{-3}	−10.90
12.3	240	26×10^3	5.17×10^{-3}	−12.03
	320	58×10^3	6.89×10^{-3}	−10.99
	400	202×10^3	8.61×10^{-3}	−9.19
14.8	160	11×10^3	2.87×10^{-3}	−12.45
	240	15×10^3	4.31×10^{-3}	−11.81
	320	23×10^3	5.74×10^{-3}	−11.18
	400	40×10^3	7.18×10^{-3}	−10.49
17.2	240	11×10^3	3.69×10^{-3}	−11.72
	320	15×10^3	4.92×10^{-3}	−11.20
	400	21×10^3	6.15×10^{-3}	−10.63
19.7	240	9×10^3	3.23×10^{-3}	−11.68
	320	11×10^3	4.31×10^{-3}	−11.16
	400	15×10^3	5.38×10^{-3}	−10.66
24.6	240	7×10^3	2.58×10^{-3}	−11.70
	320	8×10^3	3.44×10^{-3}	−11.22
	400	10×10^3	4.31×10^{-3}	−10.80
29.5	240	6×10^3	2.15×10^{-3}	−11.81
	320	7×10^3	2.87×10^{-3}	−11.31
	400	8×10^3	3.59×10^{-3}	−10.89

n_{gas} is calculated from the pressure using the ideal gas law so that

$$n_{gas} = \frac{\mathcal{V}(Z_p - 5.66\ \text{Å})p}{RT} \tag{2.6b}$$

where the value 5.66 Å represents the excluded volume, or the repulsive region near the pore walls in which no atoms are adsorbed. Thus $\mathcal{V}(Z_p - 5.66\ \text{Å})$ represents the effective volume of the pore.

Figures 1 and 2 show the calculated local energies and local chemical potentials for several pore filling values, and the local density at several pore fillings, all for the 14.8 Å pore width. Although both the local energy and the local density vary over large ranges, as one might expect for a supercritical gas adsorbed in a pore with strongly attracting walls, the local chemical potential shows only minor variations with a position inside the pore. Consequently, only the global values of the energy and chemical potential were evaluated for the other pores considered.

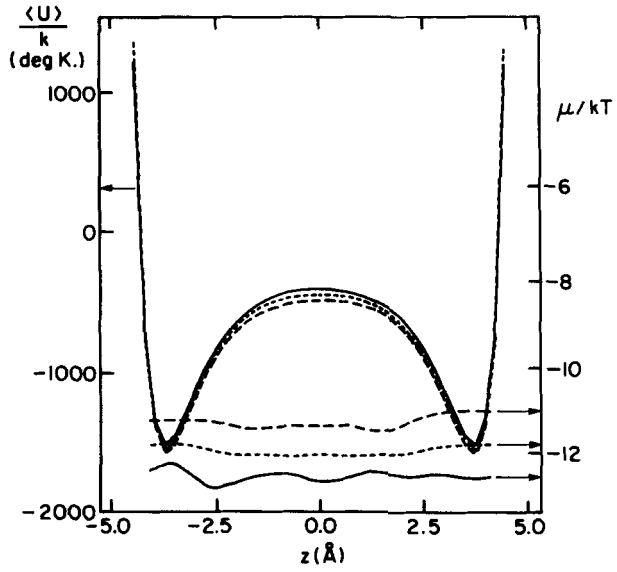

FIG. 1. Plotted here are $\langle u(z)\rangle$, the average potential energy, and $\mu(z)/kT$, the local chemical potential over kT, as a function of location within a parallel-walled slit pore of width 14.8 Å. Curves shown are for three values of pore filling: (——) $n_a/\mathcal{V} = 40 \times 10^{-3}$ molec/Å^2; (--) $n_a/\mathcal{V} = 59 \times 10^{-3}$ molec/Å^2, (– –), $n_a/\mathcal{V} = 77 \times 10^{-3}$ molec/Å^2. As expected, the local chemical potentials are nearly independent of z, while the average potential energies vary greatly, due primarily to the rapidly changing gas–solid interactions.

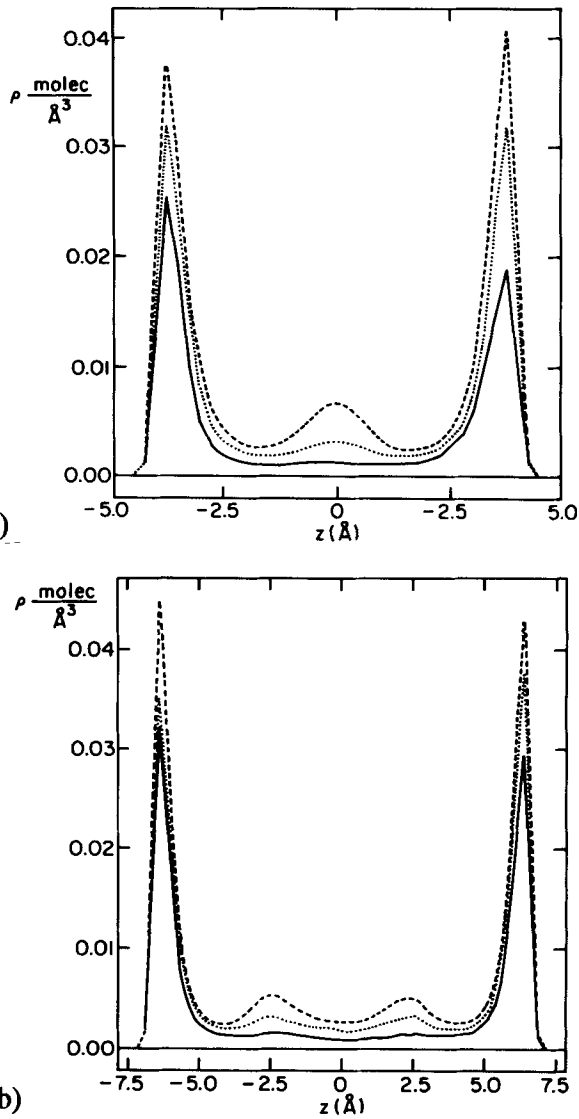

FIG. 2. In Part a, local densities are shown here for the same three systems as in Fig. 1. Note the presence of a small amount of "multilayer" adsorption for the highest pore filling value. Part b shows local densities for a wider pore with Z_p = 19.7 Å. Pore filling values are: (——), $n_a/\mathfrak{t}$ = 56 × 10^{-3} molec/Å²; (--), $n_a/\mathfrak{t}$ = 72 × 10^{-3} molec/Å²; (–·–), $n_a/\mathfrak{t}$ = 85 × 10^{-3} molec/Å². Note the presence of the central peaks at high pore fillings, corresponding to "multilayer" formation.

3. ISOTHERMS AND ADSORPTION ENERGIES

Calculated values of the Henry's law constant and the zero-coverage limiting value of the average adsorption energy change significantly as the pore dimensions and shape are altered, at least for the smaller pores. This can be seen in Figs. 3, 4, and 5 which show the variations in these quantities for parallel walls with increasing wall spacing (Fig. 3), for equilateral triangular pores with variable cross-sectional dimensions (Fig. 4), and for the isosceles triangular pores with variable apex angles for fixed cross-sectional areas (Fig. 5). In the case of parallel-walled slit pores, values of K_H and $\tilde{U}_{ms}(0)/R$ rapidly approach their limiting values for a single free surface when Z_p becomes larger than ~15 Å. In the case of the triangular pores, the variation in these parameters with pore size is slower, presumably because the strong interactions near the corners of the triangles play a large role in determining K_H and $\tilde{U}_{ms}(0)$. As pore size increases at fixed triangular shape, these interactions do not change but their contribution to the total becomes a smaller fraction of the total. The variation in K_H and $\tilde{U}_{ms}(0)$ with apex angle at fixed pore size clearly indicates that the equilateral triangle is the optimum pore shape, which is unfortunate since it seems likely that a range of angles larger than 90° is the most likely physical situation.

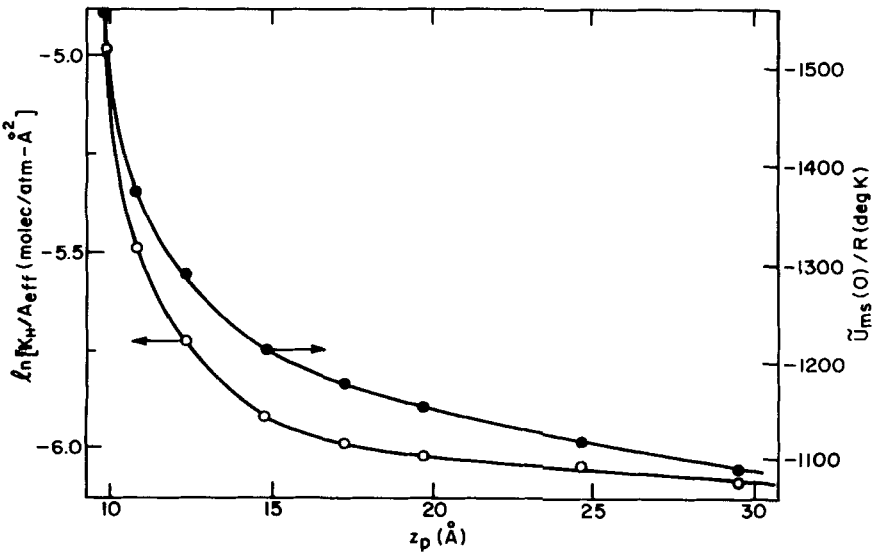

FIG. 3. The Henry's law constant K_H and the average molecule–solid interaction energy in the limit of zero coverage $\tilde{U}_{ms}(0)$ are shown here as a function of pore wall spacing Z_p for methane in parallel-walled pores at 300 K.

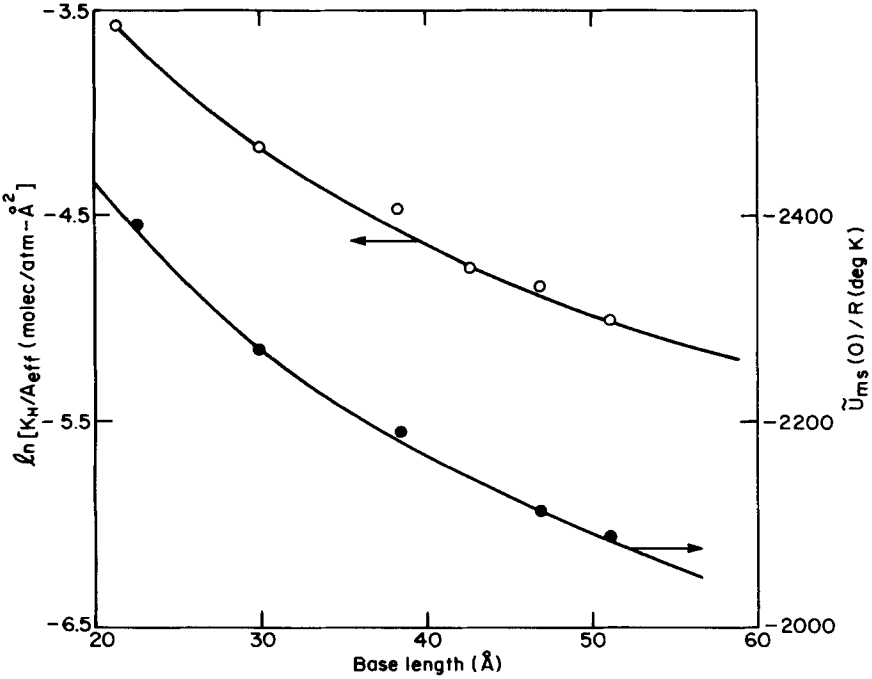

FIG. 4. Same as Fig. 3, but the data are plotted for pores of equilateral triangular cross-section but variable size, as measured by the base length of the triangle.

One somewhat surprising feature of the calculation of $U_{ms}(0)$ is the large negative values found for the triangular pores. These energies are nearly a factor of 2 larger than for the slit pores, presumably because the strong interactions in the corners of the triangles are the dominant factor in determining $\tilde{U}_{ms}(0)$ for pore sizes in the range considered here.

At finite coverage one can write $\tilde{U}_{tot}$, the average potential energy per adsorbed molecule, as

$$\tilde{U}_{tot} = \tilde{U}_{ms}(0) + \delta\tilde{U}_{ms} + \tilde{U}_{mm} \tag{3.1}$$

where $\tilde{U}_{mm}$ is the average adsorbate–adsorbate interaction per particle and $\delta\tilde{U}_{ms}$ is $\tilde{U}_{ms} - \tilde{U}_{ms}(0)$, the change in the average adsorbate–solid interaction relative to the zero coverage value $\tilde{U}_{ms}(0)$. For parallel-walled slit pores, $\delta\tilde{U}_{ms}$ is positive and, roughly, a linear function of molecules adsorbed. This is shown in Fig. 6 where it can be seen that the change is largest for the largest pores. The average methane–methane interaction energy shown in Fig. 6 is attractive (i.e., negative) and is also a roughly linear function of

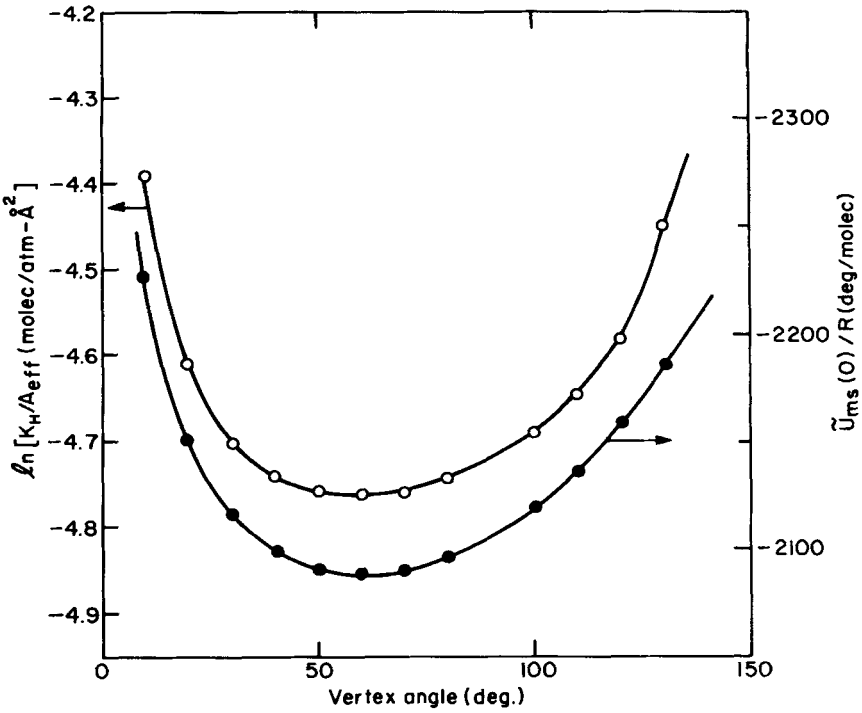

FIG. 5. Same as Fig. 3, but the data are for pores of isosceles triangular cross-section with variable vertex angle but fixed area (corresponding to a base length of 51.1 Å for a vertex angle of 60°).

coverage. The variation in this energy with pore size is not as pronounced as that for $\delta\tilde{U}_{ms}$ and is in the opposite direction.

By reference to Eq. (1.2), one sees that the dominant linear variation in both $\delta\tilde{U}_{ms}$ and $\tilde{U}_{mm}$ with coverage can be interpreted in terms of the interactions of an isolated pair of methanes with each other and with the solid. In fact, the complete expression for $\langle u_2 \rangle$ shows that it is the difference between $U(i,j,s)$ and $2U(i,s)$, where $U(i,j,s)$ denotes the average interaction of adsorbate molecules i,j with each other and with the solid, and $U(i,s)$ is the average interaction of a single molecule i with the solid. Now $U(i,j,s)$ can be decomposed into $\langle u(ij) + 2u_s(i) \rangle_{pair}$. The first of these terms contributes to the linear change in $\tilde{U}_{mm}$ with coverage, and the second, to the corresponding change in $\tilde{U}_{ms}$. However, the total linearly varying change in $\tilde{U}_{ms}$ should be written as $2\langle u_s(i) \rangle_{pair} - 2\langle u_s(i) \rangle_{single}$, where the pair and single denote the Boltzmann weight factors for two and for one molecule in the pore, i.e., exp $[(-u_s(r_i) + u_s(r_j) + u(r_{ij}))/kT]$ for the pair and exp

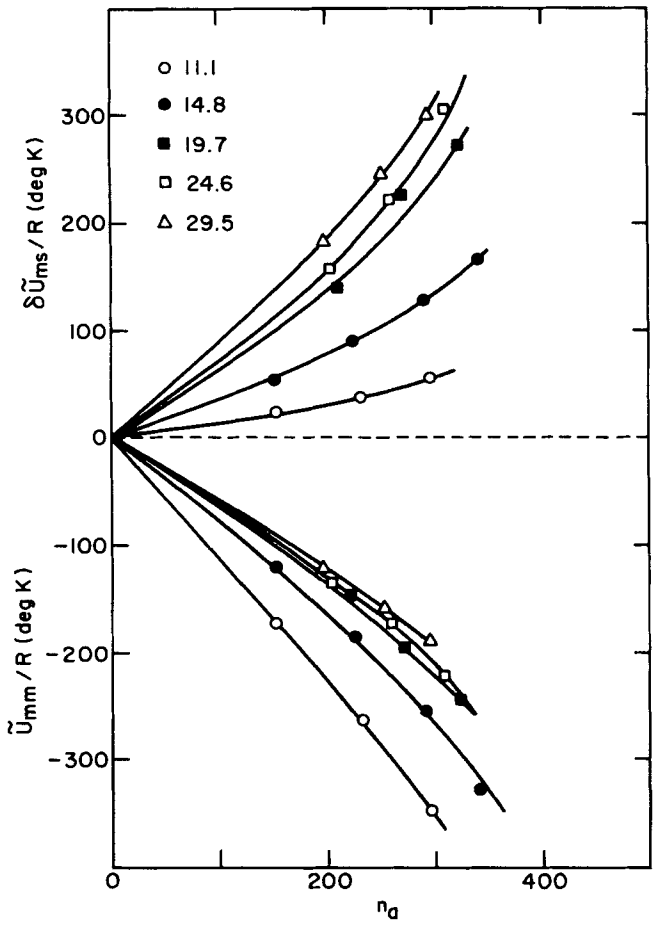

FIG. 6. Changes with pore filling n_a in the components of the average interaction energy of an adsorbed methane molecule in a parallel-walled slit pore. The data are given for a range of pore widths. (The effective volumes of these pores are listed in Table 4.)

$[-u_s(r_i)/kT]$ for the single. The physical reason for a nonzero linear variation in $\tilde{U}_{ms}$ is a consequence of the fact that these atoms are not confined to a monolayer at 300 K; that is, the exponential weighting factors are significant for a range of distances other than that for the monolayer location. One can see this in Fig. 2, which clearly shows nonzero densities for "multilayer" positions. The reason for the changes in slope with pore width in Fig. 6 is not completely clear at present, but one does know that the decay of $u_s(\mathbf{r})$ with increasing distance from the pore wall is least rapid

for the smallest pores. In effect, this means that the tendency toward simple monolayer formation weakens as the pore size decreases. The effect of this upon $U(i,j,s) - 2U(i,s)$ is not yet clear. Direct calculations of these quantities might give a definitive answer, but these are not available at present.

Although the results obtained for the changes in $\tilde{U}_{tot}$ for the triangular pores are less extensive than those for the slit pores, they are qualitatively quite similar to those for the parallel-walled slit pores. In plotting the isotherm data, one question is whether there are common features for, say, the isotherms for the parallel-walled slit pores. One way to exhibit any points of similarity is to plot $n_z/\mathcal{A}_{eff}$, the surface coverage, versus $pK_H/\mathcal{A}_{eff}$, where $\mathcal{A}_{eff}$ is the surface area available to the adsorbate. For the slit

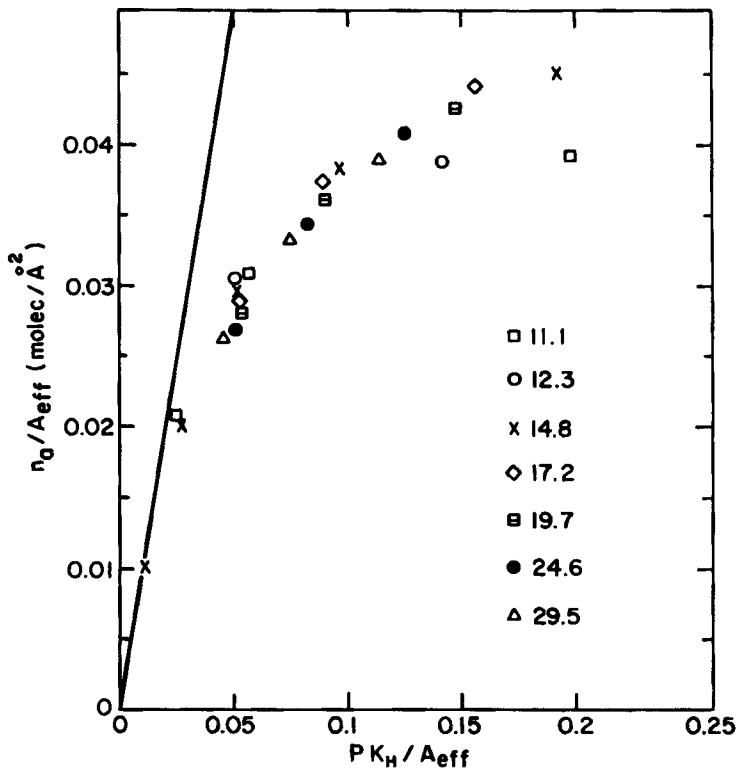

FIG. 7. Simulated isotherms for methane in slit pores of varying width are shown. The pressure is given in reduced units by multiplying by $K_H/\mathcal{A}_{eff}$ (values are plotted in Fig. 3 for these pores). The straight line gives the linear Henry's law isotherm, valid in the low coverage limit for all these systems.

pores it is equal to 2 × $\mathfrak{a}$; for the triangular pores, the effective area is calculated using an effective height and base length which are obtained by subtracting the excluded volume (~2.83 Å in width) near the walls of the pores. Such isotherms will all have initial slopes of unity and, in these coordinates, much of the influence of the changing molecule-surface potential will be removed. In fact, the family of such curves for the parallel-walled pores that is shown in Fig. 7 does define a more-or-less common curve which looks Langmuirian. However, the local densities such as those shown in Fig. 2 show clearly that these systems are not limited to monolayer formation. Consequently, fits to the Langmuir or any other monolayer isotherm serve only as interpolating functions, with values of the fitting parameter, which would be the monolayer capacity, having no physical significance.

Figure 8 shows two isotherms for selected triangular pores. A comparison with Fig. 7 shows that these plots are not much different than those for

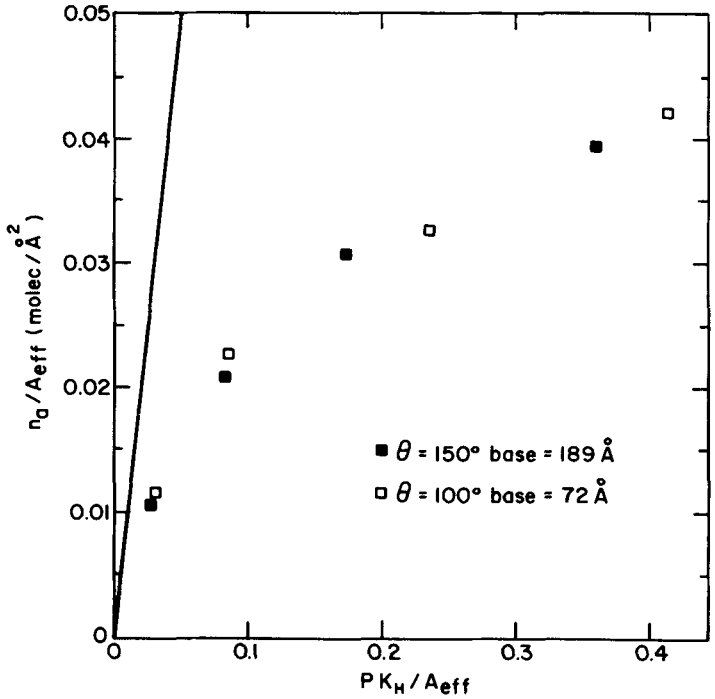

FIG. 8. Same as for Fig. 7, but for two pores of isosceles triangular cross-section with a vertex angle of 150° and a base length of 189 Å, and with a vertex angle of 100° and a base length of 71.8 Å. The two sets of data shown are for pores with nearly the same effective volume (~35,000 Å^3).

the parallel-walled pores. Of course, one expects differences to develop at very large pressure and pore filling, but this range is relatively difficult to explore for methane at 300 K, in real experiments as well as in simulations.

4. CONCLUSIONS

To this point, this paper has been concerned with presentation of a large amount of data obtained for methane adsorbed in models of microporous carbon of various pore sizes and shapes. In addition to gaining a better understanding of the microscopic behavior of this adsorption system, we can now discuss the qualifications of these systems as storage media for natural gas as an automotive fuel. In this context, a storage capacity of 12 mmol methane per cm^3 of adsorbent [i.e., 270 volumes (STP) per unit volume of adsorbent] at a pressure of 500 psi has been suggested as a viable target. The isotherms simulated in this work generally covered a range up to 900 psi, so that an interpolation using any convenient theoretical expression can be used to evaluate the total methane (adsorbed plus unadsorbed) held per unit pore volume at the target pressure. Table 4 gives the values obtained for this quantity for the pore geometries considered. In this table, effective pore volumes are tabulated as defined in Eq. (2.6b) as well as the effective surface areas. Values of n_{tar}, the interpolated value for total methane held in the pore at 500 psi, are also listed.

In order to finish the calculation, porosities of these model systems must be estimated, and this parameter obviously depends strongly upon wall thickness between pores; that is, how much carbon is present per pore. Evidently the simulations are unrelated to the choice of porosity. One knows only that the less carbon, the higher the porosity. We define porosity in the usual way: pore volume/total volume, where the total volume is the sum of pore volume plus wall volume (per pore). If one takes the basal plane separation equal to 3.4 Å, the calculation is straightforward for a given number of basal planes in the pore wall. Values of porosity and ρ_{tar}, the methane storage capacity at 500 psi and 300 K, are listed in Table 4 for two values of n_{bas} (= number of basal planes separating two pores). The value chosen initially was $n_{bas} = 3$. For this case the porosities are small and the values obtained for the methane storage are far short of what is desired. Thus, an extreme case of $n_{bas} = 1$ was considered. For such a thin wall, the simulations were rerun using the slightly weakened gas–solid potentials that characterize such systems. The limited data obtained for methane storage in such pore systems are still short of the mark but are approaching the target value for the smallest slit pores considered. None of the triangular pores was satisfactory—results listed in Table 4 are for

TABLE 4
Methane Storage at 300 K

Parallel-Walled Slits

Pore width (Å)	Effective wall spacing (Å)	Effective area (Å^2)	Effective pore volume (Å^3)	$n_{bas} = 3$			$n_{bas} = 1$		
				n_{tar} (molec)	Porosity	ρ_{tar} (mmol/cm^3)	n_{tar} (molec)	Porosity	ρ_{tar}[a] (mmol/cm^3)
11.1	5.4	7547	20,440	304	0.305	7.5	265	0.489	10.5
12.3	6.6	7547	25,070	303	0.349	7.0			
14.8	9.1	7547	34,370	312	0.424	6.4	264	0.617	7.9
17.2	11.7	7547	43,660	311	0.483	5.7			
19.7	14.0	7547	52,950	307	0.531	5.1			
24.6	18.9	7547	71,530	318	0.605	4.5			
29.5	23.7	7547	90,110	355	0.659	4.3			

Triangular Pores, $\Theta_{apex} = 60°$, $n_{bas} = 3$

Base length (Å)	Effective base length (Å)	Effective area (Å^2)	Effective pore volume (Å^3)	n_{tar} (molec)	Porosity	ρ_{tar} (mmol/cm^3)
21.3	11.5	9764	16,210	311	0.124	4.0
29.8	20.0	8720	25,200	312	0.236	4.8
38.4	28.5	7584	31,250	300	0.328	5.2
46.9	37.1	6566	35,130	278	0.404	5.3

[a]For walls that are one basal plane thick, the molecule-solid energy is slightly lower than for semi-infinite walls. Simulations were redone for $n_{bas} = 1$, and the slightly smaller n_{tar} that results is used in this calculation.

the best case for storage (equilateral triangle), even though this is believed to be physically unrealizable.

Thus, the conclusion is that the use of a pure, graphite-like porous carbon for methane storage requires extremely small slit pores that have wall spacings of a couple of molecular diameters and walls of thickness equal to one basal plane. Even in this extreme case, the target value for methane storage is not achieved. We emphasize that the simulations which bring us to this conclusion are based on intermolecular interactions that are solidly based on experimental data. It is unlikely that they are sufficiently in error to allow a reasonable expectation of a different outcome unless a physically different solid adsorbate can be devised.

Acknowledgments

This work was performed in support of the Adsorbent Enhanced Methane Storage Program at Linde Division of Union Carbide Corporation. Financial support for this program was provided by NYGAS, NYS ERDA, and GRI. Helpful discussions with Professor A. V. Vernov are gratefully acknowledged.

REFERENCES AND NOTES

1. Z. Tan and K. E. Gubbins, *J. Phys. Chem., 94,* 6061 (1990); C. Rhykerd, Z. Tan, L. A. Pozhar, and K. E. Gubbins, *Proc. Faraday Symp. 26, Molecular Transport in Confined Regions and Membranes,* Oxford, December 1990.
2. J. P. R. B. Walton and N. Quirke, *Mol. Simul., 2,* 361 (1989); M. Schoen, D. J. Diestler, and J. H. Cushman, *J. Chem. Phys., 87,* 5464 (1987); S. Sokolowski and J. Fischer, *Mol. Phys., 71,* 393 (1990); S. Sokolowski, *Ibid.,* In Press; M. Schoen, C. L. Rhykerd, J. H. Cushman and D. J. Diestler, *Ibid., 66,* 1171 (1989); A. Z. Panagiotopoulos, *Ibid., 62,* 701 (1987); J. J. Magda, M. Tirrell, and H. T. Davis, *J. Chem. Phys., 83,* 1888 (1985); Z.-B. Zhu and G. W. Robinson, *Ibid., 94,* 1403 (1991); G. Subramanian and H. T. Davis, *Mol. Phys., 38,* 1061 (1979); S. Das Sarma, K. E. Kohr, S. M. Paik, and T. R. Kirkpatrick, *Chem. Phys. Lett., 120,* 97 (1985); K. G. Honnell and C. K. Hall, *Mol. Phys., 65,* 1281 (1988); A. Yethiraj and C. K. Hall, *J. Chem. Phys., 91,* 4827 (1989); M. Moraldi and

G. Rickayzen, *Mol. Phys., 66,* 143 (1989); E. Kozak and S. Sokolowski, *J. Chem. Soc., Faraday Trans.*, In Press; W. van Megen and I. K. Snook, *Mol. Phys., 54,* 741 (1985).

3. J. M. D. MacElroy and S. H. Su, *Mol. Simul., 2,* 313 (1989); G. S. Heffelfinger, Z. Tan, K. E. Gubbins, U. B. Marconi, and F. van Swol, *Mol. Simul., 2,* 393 (1989); V. Ya Antonchenko, V. V. Ilyin, N. N. Makovsky, and V. H. Khryapa, *Mol. Phys., 65,* 1171 (1988); U. Heinbuch and J. Fischer, *Chem. Phys. Lett., 135,* 587 (1987); S. Sokolowski, *Mol. Phys.*, In Press; B. K. Peterson and K. E. Gubbins, *Ibid., 67,* 215 (1987); *J. Chem. Phys., 88,* 6487 (1988).
4. C. J. J. der Ouden, B. Smit, A. F. H. Weilers, R. A. Jackson, and A. K. Nowak, *Mol. Simul., 4,* 121 (1989); A. V. McCormick and B. F. Chemlka, *Mol. Phys., 73,* 603 (1991); T. K. Vanderlick, L. E. Scriven, and H. T. Davis, *J. Chem. Phys., 90,* 2422 (1989); J. L. Soto and A. Myers, *Mol. Phys., 42,* 971 (1981); G. B. Woods and J. S. Rowlinson, *J. Chem. Soc., Faraday Trans. 2, 85,* 765 (1989); G. B. Woods, A. Z. Panagiotopoulos, and J. S. Rowlinson, *Mol. Phys., 63,* 49 (1988); E. Cohen de Lara, R. Kahn, and A. M. Goulay, *J. Chem. Phys., 90,* 7482 (1989); S. D. Pickett, A. K. Nowak, J. M. Thomas, and A. K. Cheetham, *Zeolites, 9,* 123 (1989); R. L. June, A. T. Bell, and D. N. Theodorou, *J. Phys. Chem., 94,* 8232 (1990); P. Demontis, S. Yashonath, and M. L. Klein, *Ibid., 93,* 5016 (1989); *Chem. Phys. Lett., 153,* 551 (1988); D. M. Razmus and C. K. Hall, In Press.
5. See J. S. Rowlinson and B. Widom, *Molecular Theory of Capillarity*, Clarendon Press, Oxford, 1982, Sec. 4.2 and references listed therein.
6. See W. Steele, *The Interaction of Gases with Solid Surfaces,* Pergamon Press, Oxford, 1974, Sec. 3.6–3.8.
7. J. O. Hirschfelder, C. F. Curtiss, and R. B. Bird, *Molecular Theory of Gases and Liquids,* Wiley, New York, 1954, p. 165.
8. W. A. Steele, *Surf. Sci., 36,* 317 (1973).
9. W. A. Steele, *J. Phys. Chem., 82,* 817 (1978).
10. J. R. Sams, *J. Chem. Phys., 43,* 2243 (1965).
11. D. J. Evans and G. P. Morriss, *Chem. Phys., 77,* 63 (1983); W. G. Hoover, *Phys. Rev. A, 31,* 1695 (1985).
12. Although we use the term "pressure" here and throughout the paper, we are actually calculating the fugacity of the gas.